Pr^{3+}-DOPED STRONTIUM-ALUMINUM-BISMUTH-BORATE GLASSES FOR LASER APPLICATIONS

M. Dhamodhara Naidu [1*], Y. C. Ratnakaram [2]

[1] Rajiv Gandhi University of knowledge Technologies, IIIT-Andhra Pradesh, 516330, India; e-mail: dhamu.muppiri@gmail.com
[2] Sri Venkateswara University, Tirupathi, 517502, Andhra Pradesh, India

The chemical composition of Pr^{3+}-doped strontium-aluminum-bismuth-borate glasses with different concentrations, that is, $(50 - x)B_2O_3 + 20Bi_2O_3 + 7AlF_3 + 8SrO + 15SrF_2 + xPr_2(CO_3)_3$ (where x = 0.1, 0.5, 1.0, and 1.5 mol.%), have been prepared by the melt quenching technique. XRD, SEM, and EDS studies reveal the structural and amorphous properties of the prepared glasses. Different borate groups are analyzed by FTIR measurements. Judd-Ofelt (J-O) intensity parameters, Ω_λ (λ = 2, 4, and 6) are calculated from the absorption spectrum to identify the nature of Pr^{3+} ions with their surrounding ligands. Using the J-O parameters, the radiative properties such as radiative transition probabilities (A_R) and radiative lifetimes (τ_{cal}) are evaluated for various excited transitions of Pr^{3+} ions. Stimulated emission cross-sections (σ_p^E) and branching ratios (β_R) for the emission transitions are evaluated by the photoluminescence spectra. The higher values of σ_p^E and β_R are identified for the emission transitions $^3P_0 \rightarrow {}^3H_4$ and $^1D_2 \rightarrow {}^3H_4$ of SABiBPr15 and SABiBPr01 glasses; these glasses are suitable for light emitting materials. The chromaticity color coordinates are calculated to find the average color of the emission spectra.

Keywords: *praseodymium, optical absorption, photoluminescence, Judd-Ofelt analysis.*

СТРОНЦИЕВО-АЛЮМИНИЕВО-ВИСМУТ-БОРАТНЫЕ СТЕКЛА, ДОПИРОВАННЫЕ ИОНАМИ Pr^{3+}, ДЛЯ ПРИМЕНЕНИЙ В ЛАЗЕРАХ

M. Dhamodhara Naidu [1*], Y. C. Ratnakaram [2]

УДК 535.37;535.34;666.22

[1] Университет технологий знаний имени Раджива Ганди, IIIT-Андра Прадеш, 516330, Индия; e-mail: dhamu.muppiri@gmail.com
[2] Университет Шри Венкатешвара, Тирупати, 517502, Андра Прадеш, Индия

(Поступила 28 июня 2018)

Методом закалки в расплаве получены стронциево-алюминиево-висмут-боратные стекла, легированные ионами Pr^{3+} с различными концентрациями: $(50 - x)\ B_2O_3+20Bi_2O_3+7AlF_3+8SrO+15SrF_2+ + xPr_2\ (CO_3)_3$ (где x = 0.1, 0.5, 1.0 и 1.5 мол.%). Исследования методами XRD, SEM, EDS показывают структурные и аморфные свойства готовых стекол. Боратные группы проанализированы с помощью измерений методом FTIR. Параметры интенсивности Джадда–Офельта (J-O), Ω_λ (λ = 2, 4 и 6) рассчитаны по спектру поглощения для идентификации природы ионов Pr^{3+} с окружающими их лигандами. С помощью параметров J-O исследованы излучательные свойства (вероятности излучательных переходов (A_R) и радиационные времена жизни (τ_{cal})) для различных возбужденных переходов ионов Pr^{3+}. Сечения вынужденного излучения (σ_p^E) и соотношение ветвей распада (β_R) для переходов излучения оценены по спектрам фотолюминесценции. Более высокие значения σ_p^E и β_R получены для излучательных переходов $^3P_0 \rightarrow {}^3H_4$ и $^1D_2 \rightarrow {}^3H_4$ для стекол SABiBPr15 и SABiBPr01; эти стекла подходят для светоизлучающих материалов. Цветовые координаты цветности рассчитаны для определения среднего цвета спектров излучения.

Ключевые слова: *празеодим, оптическое поглощение, фотолюминесценция, анализ Джадда–Офельта.*

Introduction. Rare earth (RE) ion doped glasses have many advantages compared to crystalline materials, namely a wide fluorescence band due to the disordered ion environment and uniform optical properties for different glass compositions. They can be manufactured without grain boundaries and are easy for fabrication and inexpensive [1]. RE doped glass materials are useful for developing optical broad band amplifiers, solid state lasers, sensors, up-converters, and visible display device applications [2, 3]. Because of the large number of energy levels and energy level positions due to their $4f^n$ electronic configuration in the ultraviolet (UV), visible, and infrared spectral regions, RE ions have various applications [4, 5]. Compared to different glass systems, oxide glass acts as the most stable active ion host for practical applications because of its high chemical durability and thermal stability [6, 7]. The emission property of any rare earth doped glass depends on its phonon energy. In this paper, the phonon energies of B_2O_3 and Bi_2O_3 have 1400 and 500 cm^{-1}, respectively. Bi_2O_3 has a lower phonon energy than B_2O_3, and the addition of Bi_2O_3 into B_2O_3 leads to decreasing the phonon energy of the glass hosts [8]. Moreover, the fluoride content from AlF_3 also leads to decreasing the phonon energy and increasing the emission cross-sections [5].

Various applications of Pr^{3+} doped glass materials are mainly due to the large number of absorption bands in the UV, visible, and near infrared regions [9, 10]. Jamalaiah et al. [5] reported the optical absorption, fluorescence, and decay properties of Pr^{3+}-doped PbO-H_3BO_3-TiO_2-AlF_3 glasses. Murthy et al. [11] investigated the optical absorption and emission characteristics of Pr^{3+}-doped alkaline earth titanium phosphate glasses.

In this work, different concentrations of Pr^{3+} ions were doped in strontium-aluminum-bismuth-borate (SABiB) glasses, and the structural and optical properties of the obtained materials were investigated. X-ray diffraction (XRD), scanning electron microscopy (SEM), and energy dispersion spectroscopy (EDS) were used to identify the glass nature, and Fourier transform infrared (FTIR) spectroscopy was used to identify the structural groups of the SABiB glasses. The experimental oscillator strengths (f_{exp}) were calculated from the transitions of the absorption spectra, and the theoretical oscillator strengths (f_{cal}) were calculated from the Judd-Ofelt theory. Using the oscillator strengths data, the Judd-Ofelt (J-O) intensity parameters (Ω_2, Ω_4, and Ω_6) were evaluated. From the J-O intensity parameters, the radiative transition probabilities (A_R) and radiative lifetimes (τ_{cal}) were evaluated for different excited states of Pr^{3+} ions. Stimulated emission cross-sections (σ_p), branching ratios (β_R), and effective line widths ($\Delta\lambda_{eff}$) were obtained through the photoluminescence spectra for different concentrations of Pr^{3+}-doped SABiB glasses. It is observed that the present Pr^{3+} doped glass can be useful for laser emission devices.

Experimental. Trivalent praseodymium doped SABiB glasses with the composition $(50–x)B_2O_3$+ $+20Bi_2O_3+7AlF_3+8SrO+15SrF_2+xPr_2(CO_3)_3 \cdot 8H_2O$ (where x = 0.1, 0.5, 1.0, 1.5 mol.% referred to as SABiBPr01, SABiBPr05, SABiBPr10, and SABiBPr15 glasses, respectively) were prepared by the melt quenching method. The homogeneous mixture of high purity starting chemicals H_3BO_3, Bi_2O_3, AlF_3, Sr_2CO_3, SrF_2, and $Pr_2(CO_3)_3 \cdot 8H_2O$, weighing about 8 g, was thoroughly ground in an agate mortar and melted in an electric furnace at 1150°C for 45 min. This temperature was increased by 50°C as the Pr^{3+} ion concentration increased by 0.5 mol.%. During melting, the chemicals in the crucible were stirred for bubble-free and homogenous mixing. The melt was then poured onto a preheated brass plate and then pressed by another brass plate to get a uniform thickness. Finally, the glasses were annealed at 350°C for 3 h to improve the mechanical strength.

The density of the samples was measured by the Archimedes principle using xylene as the immersion liquid. The refractive indices were measured using an Abbe refractometer with a sodium vapor lamp (589.3 nm) and 1-monobromonaphthalene ($C_{10}H_7Br$) as the contact liquid. The physical parameters like thickness t, refractive index n, density ρ (g/cm^3), and concentration of rare earth ion (N, 10^{19} ions/cm^3) were calculated for 1.0 mol.% of Pr^{3+} doped SABiB glass using the formula

$$N = x\rho N_A/M,$$

where x is the mol fraction of the rare earth ion, N_A is the Avogadro number, and M is the average molecular weight or molar mass of the glass. The densities (ρ) of the glass samples were determined by the conventional Archimedes method, using xylene as the immersion liquid, with the formula

$$\rho = 0.86[a/(a - b)],$$

where a is the sample weight in air, b is the sample weight in xylene, and 0.86 gm/cm^3 is the density of xylene.

XRD patterns were obtained in the region 10-80° using an INEL C120 diffractometer with a resolution of 1° employing CoK_α radiation. We confirmed the amorphous nature of the glass sample. To analyze the surface morphology and to confirm the elemental compositions of the present SABiB glass samples, the

SEM image and the EDS spectrum were recorded using a Carl Zeiss EV0-MA15 scanning electron microscope. The FTIR spectrum was recorded using a Bruker Vertex-80 FTIR spectrophotometer in the spectral region 500–4000 cm^{-1} with a spectral resolution of 4 cm^{-1} to identify the structural groups in the glass samples. Using a Jasco V-570 spectrophotometer, the optical absorption spectral measurements were recorded in the range 420–1800 nm with a resolution of 1 nm. The excitation and emission spectra of Pr^{3+} doped glasses were recorded using a Jobin Yvon Fluorolog-3 spectrophotometer with a resolution of 1 nm by exciting with the xenon lamp at 450 nm wavelength. All the spectral measurements were carried out at room temperature.

Results and discussion. The X-ray diffraction pattern of 1.0 mol.% of Pr^{3+} doped SABiB glass is shown in Fig. 1a. No diffraction peaks were observed in the spectrum. This is the characteristic feature of the long range, disorder, which confirms that the prepared glasses are perfectly amorphous. The SEM image of 1.0 mol.% of Pr^{3+} doped SABiB glass is shown in Fig. 1b. No grains were observed in SEM images and the images were completely plain. The energy dispersive analysis of the X-rays (EDAX or EDS) spectrum of 1.0 mol.% of Pr^{3+} ion doped SABiB glass is shown in Fig. 1c. The EDS spectrum is used to find the elements of the glass sample (in %).

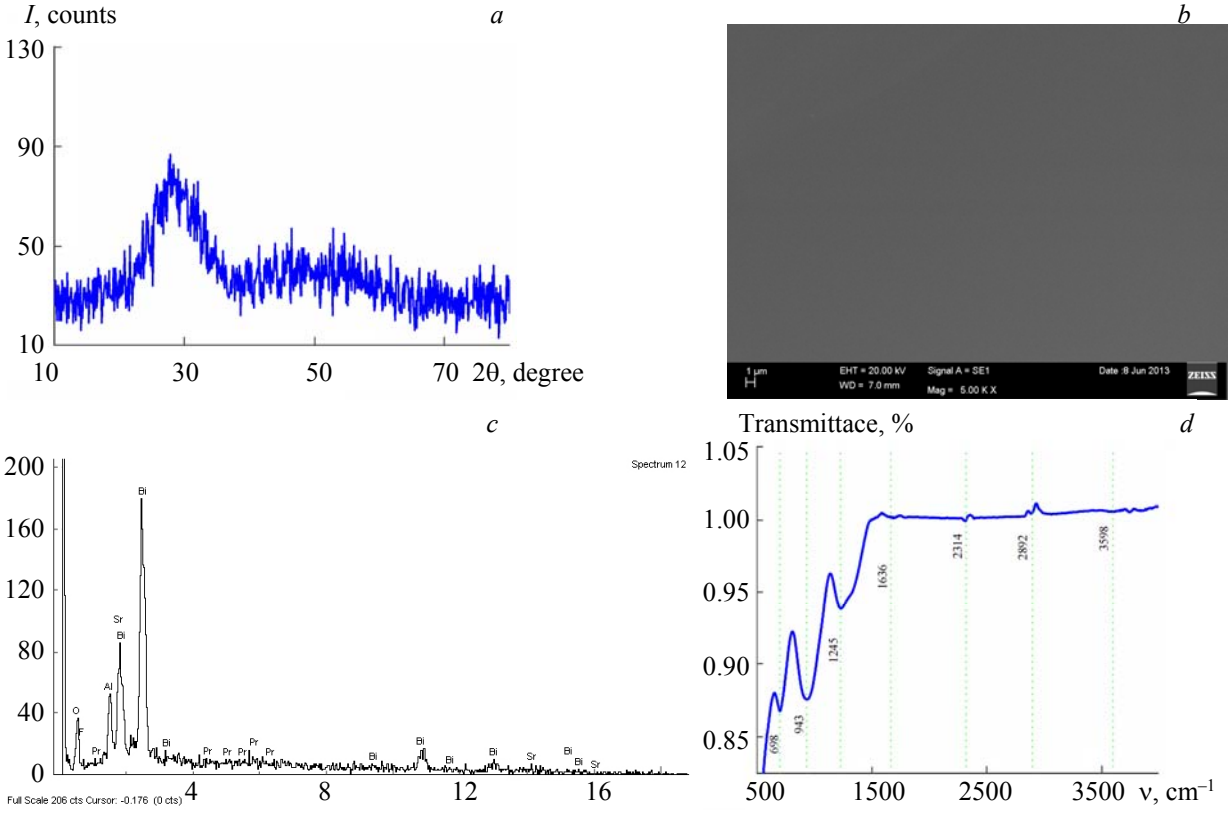

Fig. 1. XRD graph (a), SEM image (b), EDS spectrum (c), and FTIR (d) spectrum of 1.0 mol.% of Pr^{3+}-doped strontium-aluminum-bismuth-borate glass matrix

The FTIR spectrum of SABiBPr10 glass in the IR region 500–4000 cm^{-1} is shown in Fig. 1d. The observed band near 698 cm^{-1} is due to the bending vibration of the B–O–B linkage [12, 13]. One band is observed in the infrared spectral range 900–950 cm^{-1} (~ 943 cm^{-1}) and relates to the B–O stretching vibration of tetrahedral BO_4 units [14]. Another band, observed at ~1245 cm^{-1}, is due to the B–O stretching vibrations of metaborate and orthoborate groups of BO_3 units [15]. The peak around 1636 cm^{-1} can be due to the asymmetric stretching relaxation of the B–O bond of trigonal BO_3 units [16]. The peak at 2314 cm^{-1} is due to the O–H bond stretching vibrations [17]. Some peaks are observed between 2700–3600 cm^{-1}. They are due to the hydrogen bonding vibrations [18].

The optical absorption spectra for different concentrations of Pr^{3+} ion doped SABiB glasses observed in the visible and near infrared regions are shown in Fig. 2. This spectrum consists of six absorption transitions. These transitions are from the $^3H_4$ ground level to the different excited levels ($^3P_2$, $^3P_1$+$^1I_6$, $^3P_0$, $^1D_2$, $^3F_4$,

and $^3F_3$). It is observed that all these transitions occur between the $4f^2$ energy level configurations of the Pr^{3+} ions. These transitions are observed at 442, 470, 482, 589, 1446, and 1518 nm. The transitions, observed in the absorption spectrum, can be divided into three groups; one is the transition from $^3H_4 \rightarrow {}^3F_{3,4}$ in the near infrared region, the second is an isolated band related to the $^3H_4 \rightarrow {}^1D_2$ transition at 586 nm, and the third is a complex group of transitions from $^3H_4 \rightarrow {}^3P_{0,1,2}$ in the violet-blue region. Similar absorption transitions are identified in the previous works on Pr^{3+} ion doped glass materials [2, 5]. These transitions are assigned based on the reported work of Pr^{3+} ion doped glasses [19]. For Pr^{3+} ion doped glass materials, the ion has transitions $^3H_4 \rightarrow {}^3P_2$ and $^3H_4 \rightarrow {}^3F_2$, which are known as hypersensitive transitions. They obey the selection rules $\Delta S = 0$, $\Delta L \leq 2$, and $\Delta J \geq 2$ in the visible and near infrared regions, respectively. These hypersensitive transitions are strongly dependent on the interaction between the rare earth ion and neighboring ligands [20]. In the present work, the $^3H_4 \rightarrow {}^3F_2$ transition is not identified and the $^3H_4 \rightarrow {}^3P_2$ transition is only observed as a hypersensitive transition having the highest value of experimental oscillator strength in the visible region for all the concentrations.

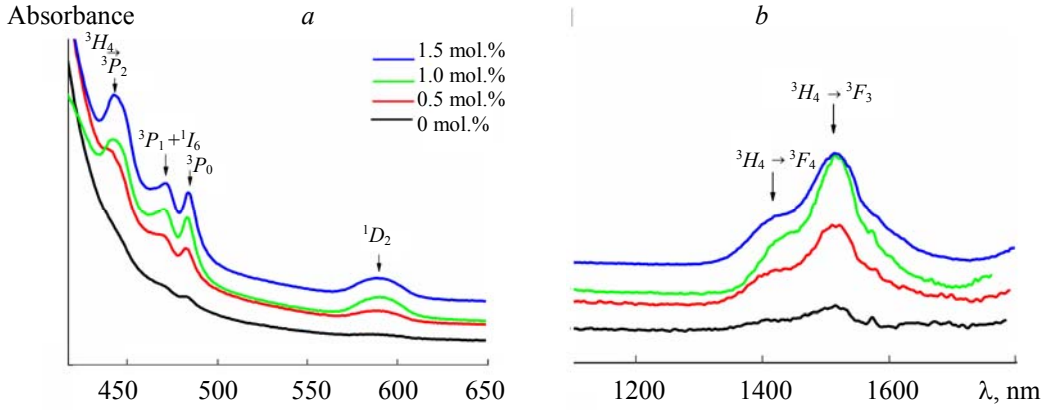

Fig. 2. UV-Vis and NIR absorption spectra of different concentrations of Pr^{3+}-doped SABiB glasses.

The experimental oscillator strengths (f_{exp}) are calculated for absorption transitions. These values directly indicate that these transitions occur from the ground state $^3H_4$ to the various excited states [5]. Experimental and calculated oscillator strengths are evaluated using the equations given by El Okr et al. [4], and the reduced matrix elements taken from the paper of Carnall et al. [19]. A good agreement between the experimental (f_{exp}) and calculated oscillator strengths (f_{cal}) is identified for the observed electric dipole transitions by the least value of the root mean square deviation as

$$\delta_{RMS} = [\Sigma(f_{exp} - f_{cal})^2/N]^{1/2},$$

where N is the total number of energy levels included in the fitting procedure. For all the concentrations, the oscillator strengths values are given in Table 1. In the present work the obtained δ_{RMS} values are almost the same for all the concentrations. The oscillator strengths and δ_{RMS} values are similar to the reported Pr^{3+} ion doped glasses [21–23]. The J-O [24, 25] intensity parameters Ω_λ ($\lambda = 2, 4, 6$) are completely host dependent, and these values are evaluated using all the absorption transitions. In the present work, the J-O intensity parameters follow the order $\Omega_6 > \Omega_2 > \Omega_4$ for all the concentrations, and these values are compared with the reported work of Pr^{3+} ion doped glasses given in Table 2. The covalency of the rare earth ion with the surrounding ligands is proportional to the value of Ω_2 parameter. The higher value of the Ω_2 parameter is observed for SABiBPr01 glass, indicating the stronger covalent bonding and lower site symmetry of the rare earth ion with the surrounding ligands. The Ω_4 and Ω_6 parameters are considered as indicators of the viscosity of the Pr^{3+} doped glasses [26]. The stimulated emission in a laser active medium is estimated by the spectroscopic quality factor (χ), which is the ratio of the Ω_4 and Ω_6 parameters [27]. The higher spectroscopic quality factor (χ) of the host materials indicates the promised stimulated emission. SABiBPr10 and SABiBPr15 glasses have higher values of χ, indicating that their stimulated emissions are higher compared to the other two glasses in the present work. The χ values of the present glasses are lower than the χ values of all the reported Pr^{3+} ion doped glasses [9, 28–30] and are similar to phosphate glasses [30]. These comparisons are shown in Table 2.

TABLE 1. Experimental oscillator strengths (f_{exp}) and calculated oscillator strengths (f_{cal}) in certain excited states of Pr^{3+}-doped strontium-aluminum-bismuth-borate glasses for all the concentrations

$^3H_4\rightarrow$	0.1 mol.%		0.5 mol%		1.0 mol%		1.5 mol%	
	f_{exp}	f_{cal}	f_{exp}	f_{cal}	f_{exp}	f_{cal}	f_{exp}	f_{cal}
$^3P_2$	13.08	9.30	13.57	9.42	13.70	8.98	13.79	7.56
$^3P_1+^1I_6$	3.13	4.41	2.96	4.41	3.38	4.65	2.65	3.95
$^3P_0$	3.61	2.08	3.71	2.1	3.5	2.3	2.79	2.0
$^1D_2$	4.00	2.83	4.27	2.85	4.42	2.72	3.11	2.30
$^3F_4$	10.09	10.04	10.16	10.15	9.57	9.64	7.82	8.12
$^3F_3$	15.07	14.97	15.14	15.10	14.65	14.55	12.48	12.28
δ_{RMS}	±2.708		±2.827		±3.0465		±3.739	

TABLE 2. Judd-Ofelt intensity parameters ($\Omega_\lambda\times10^{-20}$ cm^2) (λ =2, 4, and 6) and spectroscopic quality factors (χ) for all the concentrations of Pr^{3+}-doped SABiB glasses

Glass	Ω_2	Ω_4	Ω_6	$\Sigma\Omega_\lambda$	$\chi = \Omega_4/\Omega_6$	Trend	Reference
SABiBPr01	5.85	3.19	15.79	24.83	0.21	$\Omega_6 > \Omega_2 > \Omega_4$	Present work
SABiBPr05	5.17	3.19	15.95	24.31	0.20	$\Omega_6 > \Omega_2 > \Omega_4$	Present work
SABiBPr10	5.37	3.56	15.12	24.05	0.24	$\Omega_6 > \Omega_2 > \Omega_4$	Present work
SABiBPr15	5.19	3.02	12.70	20.91	0.24	$\Omega_6 > \Omega_2 > \Omega_4$	Present work
Zinc chlorideborophosphate	3.72	3.31	5.38	12.41	0.62	$\Omega_6 > \Omega_2 > \Omega_4$	[9]
Lead borate	3.59	3.50	5.26	12.35	0.67	$\Omega_6 > \Omega_2 > \Omega_4$	[28]
Chlorophosphate	4.38	1.86	4.15	10.39	0.45	$\Omega_2 > \Omega_6 > \Omega_4$	[29]
Phosphate	10.0	2.0	7.0	19	0.29	$\Omega_2 > \Omega_6 > \Omega_4$	[30]

Figure 3a represents the excitation spectrum of SABiBPr10 glass, measured by monitoring an intense emission at 617 nm. From the excitation spectrum, excitation peaks are observed and these are assigned to the electronic transitions, $^3H_4\rightarrow{}^3P_2$, $^3H_4\rightarrow{}^3P_1$, and $^3H_4\rightarrow{}^3P_0$ at 450, 471, and 485 nm, respectively. Among these transitions, the highest intensity transition wavelength (450 nm) is selected for emission spectral measurements. Figure 3b shows the emission spectra of different concentrations of the Pr^{3+} ion doped SABiB glasses obtained upon excitation with 450 nm in the wavelength range 450–700 nm. The emission profiles are found to be the same but variations of peak intensities are observed while the rare earth ion concentration is changed. The emission mechanism for the SABiBPr10 glass matrix is shown in Fig. 4.

Initial radiation excites Pr^{3+} ions from the $^3H_4$ ground state to the $^3P_2$ level and then, due to nonradiative transitions, these ions move from $^3P_2$ to the metastable states $^3P_1+^1I_6$, $^3P_0$, and $^1D_2$. Finally, the emission takes place from these metastable states to different lower levels $^3H_4$, $^3H_5$, and $^3F_2$. In the emission spectra, four emission bands are observed around 491, 532, 612, and 648 nm, and these bands are assigned to the transitions $^3P_0\rightarrow{}^3H_4$, $^3P_1\rightarrow{}^3H_5$, $^1D_2\rightarrow{}^3H_4$, and $^3P_0\rightarrow{}^3F_2$, respectively. The emission band positions are assigned following Jamalaiah et al. [5]. The emission transitions $^3P_0\rightarrow{}^3H_4$ and $^1D_2\rightarrow{}^3H_4$ are more intensive-compared to other transitions. The fluorescence intensity of the transition $^3P_0\rightarrow{}^3H_4$ increases with increasing

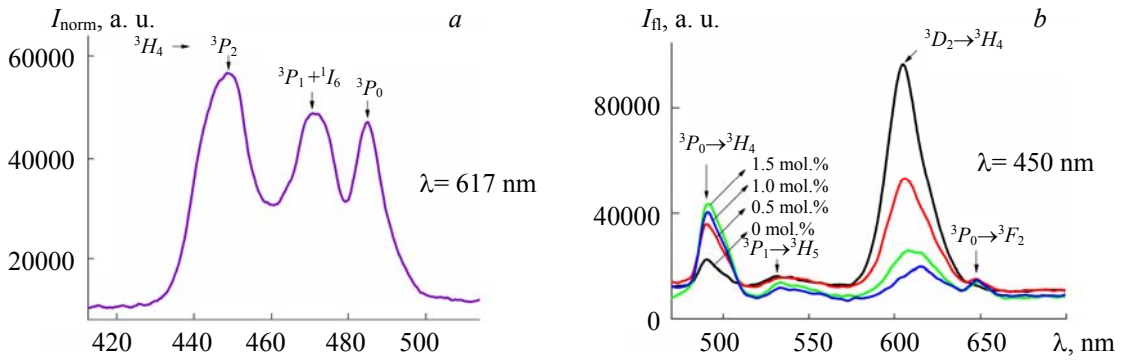

Fig. 3. Excitation spectrum of 1.0 mol% of Pr^{3+} (a) and emission spectra for all the concentrations of Pr^{3+}-doped SABiB glasses (b).

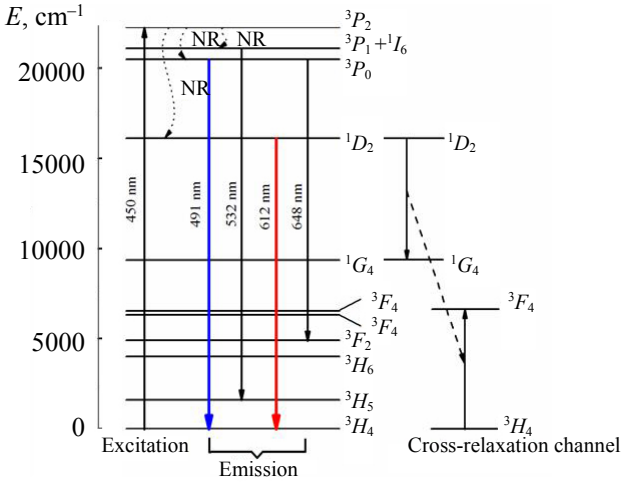

Fig. 4. Energy level diagram for emission mechanism of 1.0 mol.% of Pr^{3+}-doped SABiB glass.

Pr^{3+} ions concentration up to 1.0 mol.% and then decreases for 1.5 mol.% due to the concentration quenching of the emission intensity by the large energy transfer between Pr^{3+} ions. This is the optimized concentration of Pr^{3+} ions for the $^3P_0 \rightarrow {}^3H_4$. The fluorescence intensity of the $^1D_2$ emitting level is dominant at 0.1 mol.% because this state is populated by fast multiphonon non-radiative relaxation from the higher lying $^3P_{0-1}$ level. The intensity decreases of $^1D_2$ level at higher concentrations (>0.5 mol.%) is due to the energy transfer through the cross-relaxation channel. Therefore, due to the cross-relaxation, the fast quenching in emission intensity takes place.

The increase in the Pr^{3+} ion concentration results in a significant red shift in the emission transition $^1D_2 \rightarrow {}^3H_4$. This shift may be ascribed to the site distribution of Pr^{3+} ions in the vicinity of ligand fields [31]. For different Pr^{3+} ion concentrations (0.1, 0.5, 1.0, and 1.5 mol.%) of the represented glasses, the transition $^1D_2 \rightarrow {}^3H_4$ is observed at 604, 608, 612, and 617 nm, respectively. The redshift can be identified as the fixed difference in the wavelength of the emission transition with increasing concentration of the Pr^{3+} ion. However, for other three emission transitions ($^3P_0 \rightarrow {}^3H_4$, $^3P_1 \rightarrow {}^3H_5$, and $^3P_0 \rightarrow {}^3F_2$), the redshift is not observed. Using the J-O intensity parameters, the radiative parameters (like radiative transition probability (A_R), peak stimulated emission cross-section (σ_P^E), branching ratios (β_{exp} and β_{cal}), and integrated absorption cross-section (Σ)) are calculated for certain excited states of Pr^{3+} ion doped SABiB glasses. The branching ratio (β) is an important radiative parameter that can be calculated as the ratio of radiative transition probability (A_R) for a transition from the excited state to a lower state and the total radiative transition probability (A_T) of the excited state; here A_T is the sum of the A_R terms for all the transitions. Branching ratio values are calculated using the equation given by Zhang et al. [2]. The radiative lifetimes of $^3P_0$ state are calculated from the total radiative transition probabilities. These values are 19.21, 20.12, 19.40, and 21.87μs for 0.1, 0.5, 1.0, and 1.5 mol.% of Pr^{3+} ion doped glasses, respectively. From Table 3 it follows that the transition $^3F_3 \rightarrow {}^3H_4$ has higher branching ratios, and the $^3P_0 \rightarrow {}^3F_2$ transition has higher absorption cross-sections for all the concentrations.

The higher values of experimental branching ratios (β_{exp}) are obtained from the areas under the emission bands. The transitions having higher branching ratios are of interest for laser application. In the present work β_{exp} values are compared with β_{cal} for all the concentrations. The variations in the values of branching ratios with increase of the ion concentration for the emission transitions $^3P_0 \rightarrow {}^3H_4$ and $^1D_2 \rightarrow {}^3H_4$ are similar to the branching ratio values reported by Jamalaiah et al. [5], and these values are presented in Table 4. Based on the values of branching ratios and data of the emission spectrum, it is observed that the two emission transitions $^3P_0 \rightarrow {}^3H_4$ and $^1D_2 \rightarrow {}^3H_4$ have dominant intensities at different concentrations and are confirmed as laser transitions.

In the present work, chromaticity coordinates are calculated for all the Pr^{3+}-doped glass matrices, and these coordinates are characterized by the CIE colorimetric standards (they are used by Smith and Guild [32], for example). The chromaticity coordinate values are (0.53, 0.42), (0.47, 0.44), (0.42, 0.46), and (0.38, 0.45) for 0.1, 0.5, 1.0, and 1.5 mol.% of Pr^{3+} doped SABiB glass matrices, respectively. For all the concentrations of Pr^{3+} doped glass matrices, the coordinate values fall in the yellow region, as shown

in Fig. 5. As the concentration increases from 0.1 to 1.5 mol.%, the chromaticity coordinate values move towards the green region. Hence, from the chromaticity diagram it is evident that for all the Pr^{3+}-doped SABiB glasses the average emission color is yellow.

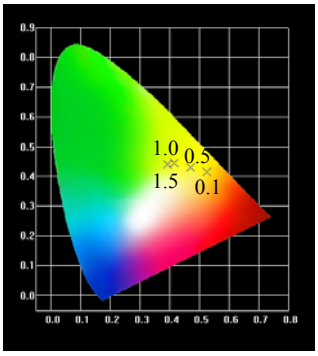

Fig. 5. CIE color coordinate diagram of different concentrations of Pr^{3+}-doped SABiB glasses with excitation wavelength 450 nm.

TABLE 3. Branching ratios (β) and integrated absorption cross-sections ($\sum \cdot 10^{18}$ cm^{-1}) of Pr^{3+}-doped SABiB glasses (for all the concentrations)

Transition	0.1 mol.%		0.5 mol.%		1.0 mol.%		1.5 mol.%	
	β	Σ	β	Σ	β	Σ	β	Σ
$^3P_1 \rightarrow {}^3F_3$	0.24	28.13	0.23	25.35	0.23	26.63	0.25	25.18
$^3P_1 \rightarrow {}^3H_6$	0.18	15.91	0.19	16.08	0.17	15.22	0.16	12.8
$^3P_1 \rightarrow {}^3H_5$	0.30	21.22	0.32	21.34	0.31	21.61	0.30	18.24
$^3P_0 \rightarrow {}^3F_2$	0.37	38.81	0.34	34.22	0.34	35.51	0.37	34.33
$^3P_0 \rightarrow {}^3H_6$	0.28	26.94	0.30	27.17	0.27	25.73	0.26	21.62
$^3P_0 \rightarrow {}^3H_4$	0.28	16.55	0.29	16.52	0.35	18.42	0.30	15.63
$^1D_2 \rightarrow {}^3F_4$	0.36	11.19	0.33	9.97	0.34	10.25	0.37	9.84
$^1D_2 \rightarrow {}^3H_4$	0.41	4.5	0.43	4.52	0.41	4.33	0.39	3.66
$^3F_3 \rightarrow {}^3H_4$	0.88	16.58	0.88	17.11	0.88	16.53	0.88	13.95

TABLE 4. Emission band positions (λ_P), effective line widths ($\Delta\lambda_{eff}$), radiative transition probabilities (A_R), peak stimulated emission cross-sections (σ_P), and branching ratios (β) of Pr^{3+}-doped SABiB glasses (for all the concentrations)

Transition	Parameter	0.1 mol.%	0.5 mol.%	1.0 mol.%	1.5 mol.%
$^3P_0 \rightarrow {}^3H_4$	λ_P, nm	490.5	490.5	491.2	491
	$\Delta\lambda_{eff}$, nm	39.1	23.9	16.9	19.5
	A_R, s^{-1}	14688	14629	16293	13831
	σ_P, 10^{-20} cm^2	6.73	4.10	3.23	3.16
	β_{cal}	0.28	0.29	0.35	0.30
	β_{exp}	0.06	0.21	0.45	0.47
$^1D_2 \rightarrow {}^3H_4$	λ_P, nm	604	608	612	617
	$\Delta\lambda_{eff}$, nm	15.8	16.2	17.2	20.9
	A_R, s^{-1}	2681	2685	2568	2179
	σ_P, 10^{-20} cm^2	0.76	0.78	0.81	0.84
	β_{cal}	0.41	0.43	0.41	0.39
	β_{exp}	0.89	0.69	0.41	0.34

Conclusion. The absorption and emission properties of Pr^{3+}-doped strontium-aluminum-bismuth-borate glasses are studied. The amorphous nature of the studied glass matrix is confirmed by the XRD spectrum and the SEM image. The presence of the elements in the glass sample is confirmed by the EDS spectrum. Different structural groups are identified by the FTIR spectrum. In the determination of the J-O intensity parame-

ters, the small δ_{RMS} deviations show a good agreement between the experimental and calculated oscillator strengths, including the $^3H_4 \rightarrow {}^3P_2$ hypersensitive transition. A higher value of the Ω_2 parameter is observed for SABiBPr01 glass, indicating stronger covalent bonding and lower site symmetry of the rare earth ion with the surrounding ligands. The spectroscopic quality factor ($\chi = \Omega_4/\Omega_6$) is higher for both SABiBPr10 and SABiBPr15 glasses, indicating their high stimulated emissions. The two emission transitions $^3P_0 \rightarrow {}^3H_4$ and $^1D_2 \rightarrow {}^3H_4$ have dominant intensities for all the concentrations, which confirms their prospects for laser application. The average color of the emission spectrum is found to be yellow, and it is confirmed by the chromaticity color coordinate diagram.

REFERENCES

1. M. P. Hehlen, N. J. Cockcroft, T. R. Gosnell, A. J. Bruce, G. Nykolak, J. Shmulovich, *Opt. Lett.*, **22**, 772–774 (1997).
2. Y. Y. Zhang, B. J. Chen, E. Y. B. Pun, H. Lin, *Physica B*, **404**, 1132–1136 (2009).
3. H. J. Lozykowski, W. M. Jadwisienczak, I. Brown, *J. Appl. Phys*., **88**, 210–222 (2000).
4. M. El Okr, M. Farouk, M. El-Sherbiny, M. A. K. El-Fayoumi, M. G. Brik, *J. Alloys Compd*., **490**, 184–189 (2010).
5. B. C. Jamalaiah, J. Suresh Kumar, A. Mohan Babu, L. Rama Moorthy, Kiwan Jang, Ho Sueb Lee, M. Jayasimhadri, Jung Hyun Jeong, Hyukjoon Choi, *J. Lumin*., **129**, 1023–1028 (2009).
6. J. L. Doualan, S. Girard, H. Haquin, J. L. Adam, J. Montagne, *Opt. Mater*., **24**, 563–574 (2003).
7. H. Lin, K. Liu, E. Y. B. Pun, T. C. Ma, X. Peng, Q. D. An, J. Y. Yu, S. B. Jiang, *Chem. Phys. Lett*., **398**, 146–150 (2004).
8. Shiqing Xu, Zhongmin Yang, Shixun Dai, Guonian Wang, Lili Hu, Zhonghong Jiang, *J. Non-Cryst. Solids*, **347**, 197-203 (2004).
9. Y. K. Sharma, S. P. Tondon, S. S. L. Surana, *Mater. Sci. Eng. B*, **77**, 167-171 (2000).
10. Y. C. Ratnakaram, A. V. Kumar, D. T. Naidu, N. O. Gopal, *Mater. Lett*., **58**, 3908–3914 (2004).
11. D. V. R. Murthy, B. C. Jamalaiah, T. Sasikala, L. Rama Moorthy, M. Jayasimhadri, *Physica B*, **405**, 1095–1100 (2010).
12. E. I. Kamitsos, A. P. Patsis, M. A. Karakassides, G. D. Chryssikos, *J. Non-Cryst. Solids*, **126**, 52–67 (1990).
13. A. K. Hassan, L. Borjesson, L. M. Torell, *J. Non-Cryst. Solids*, **154**, 172–174 (1994).
14. G. El-Damrawi, K. El-Egili, *Physica B*, **299**, 180–186 (2001).
15. B. Karthikeyan, S. Mohan, *Physica B*, **334**, 298–302 (2003).
16. G. Lakshminarayana, S. Buddhudu, *Spectrochim. Acta A*, **62**, 364–371 (2005).
17. B. H. Rudramadevi, S. Buddhudu, *Indian J. Pure Appl. Phys*., **46**, 825–832 (2008).
18. S. G. Motke, S. P. Yawale, S. S. Yawale, *Bull. Mater. Sci*., **25**, 75–78 (2002).
19. W. T. Carnall, P. R. Fields, K. J. Rajnak, *J. Chem. Phys*., **49**, 4412 (1968).
20. C. K. Jorgensen, B. R. Judd, *Mol. Phys*., **8**, 281–290 (1964).
21. Z. Mazurak, S. Bodyl, R. Lisiecki, J. Gabryś-Pisarska, M. Czaja, *Opt. Mater*., **32**, 547–553 (2010).
22. K. Venkata Rao, Y. C. Ratnakaram, M. Seshadri, J. L. Rao, *Physica B*, **405**, 2297–2304 (2010).
23. L. Srinivasa Rao, J. Venkatappa Rao, P. Syam Prasad, *IOP Conf. Series: Mater. Sci. Eng*., **2**, 012025 (2009).
24. B. R. Judd, *Phys. Rev*., **127**, 750–761 (1962).
25. J. S. Ofelt, *J. Chem. Phys*., **49**, 4774–4780 (1962).
26. *Handbook on the Physics and Chemistry of Rare Earths*, Eds. R. Reisfeld, C. K. Jorgensen, K. A. Gschneidner Jr., L. Eyring, **9**, Ch. 58, North Holland, Amsterdam (1987).
27. A. A. Kaminskii, *Laser Crystals*, Berlin, Springer (1990).
28. S. A. Saleem, B. C. Jamalaiah, M. Jayasimhadri, A. Srinivasa Rao, Kiwan Jang, L. Rama Moorthy, *J. Quant. Spectrosc. Radiat. Transfer*, **112**, 78–84 (2011).
29. K. Subramanyam Naidu, S. Buddhudu, *J. Mater. Sci. Lett*., **11**, 386 (1992).
30. *Handbook on the Physics and Chemistry of Rare Earths*, Eds. K. A. Gschneidner, Jr., L. Eyring, **25**, Elsevier Science B.V (1998).
31. X. J. Wang, H. R. Zheng, D. Jia, S. H. Huang, R. S. Meltzer, M. J. Dejneka, W. M. Yen, *Microelectronics*, **34**, 549–551 (2003).
32. T. Smith, J. Guild, *Trans. Opt. Soc*., **33**, 103–105 (1931).